Correlation between resistivity and oxygen vacancy of hydrogen-doped indium tin oxide thin films

Koichi Okada,[a] Shigemi Kohiki,[a,*] Suning Luo,[a,b] Daiichiro Sekiba,[c] Satoshi Ishii,[c] Masanori Mitome,[d] Atsushi Kohno,[e] Takayuki Tajiri,[e] and Fumiya Shoji[f]

[a]*Department of Materials Science, Kyushu Institute of Technology, 1-1 Sensui, Tobata, Kitakyushu 804-8550, Japan*

[b]*Liaoning Institute of Technology, No.169 Shiying Street, Jinzhou 121001, Liaoning, China*

[c]*Tandem Accelerator Complex, University of Tsukuba, 1-1-1 Tennodai, Tsukuba, Ibaraki 305-8577, Japan*

[d]*National Institute for Materials Science, 1-1 Namiki, Tsukuba, Ibaraki 305-0044, Japan*

[e]*Department of Applied Physics, Fukuoka University, 8-19-1 Nanakuma, Jonan, Fukuoka 814-0180, Japan*

[f]*Kyushu Kyoritsu University, 1-8 Jiyugaoka, Yahatanishi, Kitakyushu 807-8585, Japan*

ABSTRACT

Thin films of indium tin oxide (ITO) sputter-deposited by *dc*-plasma containing deuterium on glass substrate without any heat treatments exhibited gradual lowering in electrical resistivity with increasing the deuterium content [D_2] in plasma gas by 1 %, and then demonstrated a jump in resistivity by further increase of [D_2] than 1 %. X-ray photoelectron spectroscopy revealed that hydroxyl-bonded oxygen in ITO grew continuingly with [D_2]. Deuterium positioned at the interstitial site increased almost quantitatively with increasing [D_2]. Rutherford backscattering spectroscopy showed gradual reduction in the oxygen content of ITO with increasing [D_2] by 1 %, and then demonstrated an abrupt increase of the oxygen content with the increase of [D_2] than 1 %. The films with [D_2] < 1 % were oxygen deficient but those with [D_2] > 1 % were excess of oxygen. The most oxygen deficient film of [D_2] = 1 % was the most conductive. Behavior in the resistivity with [D_2] looks parallel to that in the oxygen content. A lower resistivity of the films corresponded well to oxygen vacancy rather than hydrogen interstitial.

KEYWORDS: ITO thin film, oxygen vacancy, hydrogen interstitial, x-ray photoelectron spectroscopy, Rutherford backscattering spectroscopy

1. INTRODUCTION

In the energy-conversion research field, hydrogen incorporation to thin films of indium sesquioxide (In_2O_3) is now of interest for achieving higher conductivity with higher transparency in near-infrared wavelength region [1]. In_2O_3 is known to crystallize into the *C*-type rare-earth structure. Indium atoms occupy Wyckoff positions 8b and 24d, and oxygen atoms occupy Wyckoff position 48e. Each oxygen atom forms distorted tetrahedral bonds with its neighboring indium atoms (one In atom at the 8b position and three In atoms at the 24d position), as shown by the upper panel of Fig. 1. Hydrogen incorporated In_2O_3 films, prepared by *rf*-magnetron sputtering with water vapor introduced into a deposition chamber, demonstrated that carriers of the films deposited without substrate heating were originated from doubly charged impurities, while those of the films annealed at 200 ^oC for 2 h in vacuum were resulted from singly charged impurities [1]. Muonium was reported to form a shallow donor center in In_2O_3 with the activation energy of 47 ± 6 meV [2]. Hydrogen is reported to behave as a shallow donor in In_2O_3, and oxygen vacancy is not responsible for free carriers [2,3]. The first-principles calculation also revealed that hydrogen located at the interstitial site (the middle panel of Fig. 1) and that substituted for the oxygen site of In_2O_3 are shallow donors [4]. The oxygen vacancies (the lower panel of Fig. 1) in both the 2+ charged and neutral states are stable, although the oxygen vacancy in the 1+ charged state is never stable in In_2O_3 [4].

Even in the electronic device industry, hydrogen treatment is promising for lowering resistivity of indium tin oxide (ITO) thin film for next-generation device applications using organic substrates [5]. Thin film deposition without substrate heating tends to result in amorphousness in crystallinity. In amorphous ITO oxygen vacancy can be the primary source of charge carriers, because tin is not efficiently activated [6]. Oxygen vacancy has been believed to play the role of doubly charged donor in In_2O_3 [7,8]. Metallic conductivity due to oxygen vacancy was reported for vacuum annealed In_2O_3 film [9] and for pulsed-laser deposited ITO films grown at oxygen pressures lower than 1×10^{-2} Pa [10]. A high conductivity was reported for hydrogen incorporated ITO film deposited by *dc*-plasma

sputtering with a mixed gas of argon and deuterium [11]. Because hydrogen radical generated in plasma is a strong reducing species [12], hydrogen can withdraw oxygen from the crystal during the deposition as shown in the lower panel of Fig. 1, and then bring about oxygen vacancy playing the role of double donor in the film.

On the other hand, hydrogen atoms can be incorporated in solid film when they occupy the interstitial site of the crystal, as shown in the middle panel of Fig. 1. The residing hydrogen forms hydroxyl bond [13] which is expected to play the role of scattering center for charge carriers. Hydroxyl-bonded oxygen gives rise to the suboxide-like O 1s peak appearing at the higher-binding energy side than the peak due to lattice-oxygen in x-ray photoelectron spectroscopy (XPS). We examined growths of the hydroxyl-bonded oxygen peak with the deuterium concentration in plasma gas by using XPS. In the hydrogen incorporated ITO film, the hydrogen interstitial became denser in proportion to the deuterium concentration in the plasma. It is well known that oxygen and others can be simultaneously quantified by Rutherford backscattering spectroscopy (RBS) [14-18]. Variation in the atomic ratio of oxygen to the sum of indium and tin with the deuterium concentration in the plasma was also examined by using RBS. Change in electrical resistivity with the deuterium concentration looks parallel to that in the oxygen content by RBS. We found that lower resistivity for the film corresponds to denser oxygen vacancy rather than richer hydrogen interstitial.

2. EXPERIMENT

In *dc*-plasma of mixed gas of argon and deuterium, ITO films were grown on glass substrate by sputtering of a sintered target (Kojundo Chemical, Japan) without intentional substrate heating. The sputtering-target consisted of In_2O_3 (95 wt. %) and SnO_2 (5 wt. %). The excitation conditions of plasma were as follows: gas pressure of $\approx 1.3 \times 10^{-1}$ Pa, anode voltage of 75 V, and an anode current of 0.8 A. Argon gas (99.9999 % purity) and deuterium gas (99.99 % purity) were introduced to deposition chamber with the base pressure of $\approx 1.3 \times 10^{-5}$ Pa. It is well known that protium related species such as H_2 and H_2O molecules are usually involved in the residual gas of vacuum systems. The ITO films were deposited at the partial pressure of deuterium gas ranging from $\approx 1.3 \times 10^{-5}$ to 4.8×10^{-3} Pa. The gas pressure ratio of deuterium to argon, denoted as the deuterium gas concentration [D_2] in the deposition,

was in the range from 0 to 3.6 %. The film thickness reached to ≈200 nm by the deposition of 120 min. Post-deposition heating in air of the films were eliminated to scrutinize changes in both the concentration of deuterium resided in and that of oxygen vacancy of the film in relation to the [D_2] value.

Transmission electron microscopy (TEM) for cross-sectioned specimens was carried out using a JEOL JEM-3100FEF operated at the electron acceleration voltage of 300 kV. Energy dispersive x-ray spectrometer attached on the TEM was used for elemental distribution analysis. XPS was carried out using a ULVAC-PHI model-1800L with monochromatized Al *K*α radiation in vacuum pressure less than 6.5×10^{-7} Pa. The spectrometer was calibrated by using the Au $4f_{7/2}$ (84.0 eV) electrons. The estimated electron energy uncertainty was ±0.15 eV in this experiment. All the samples were highly conductive. Oxygen vacancy in the samples was quantified by RBS method using the Tandem Accelerator installed at Tandem Accelerator Center in University of Tsukuba, Japan. Ions of He^{2+} accelerated up to 2.5 MeV were injected at the angle of 15^o to the sample surface. The back-scattered ions were collected by the detectors set at the angle of 150^o with respect to the beam direction [19].

3. RESULTS and DISCUSSION

Cross-sectional TEM images (Fig. 2) indicate that film thickness of the samples with [D_2] ≤ 1.5 % was ≈160 nm and that with [D_2] = 3.6 % was ≈110 nm. As shown by the insets of Fig. 2, electron diffraction revealed that all the samples are polycrystalline. Diffuse diffracted rings overlapping with diffracted spots were consistent with x-ray diffraction (not shown) using a Rigaku CN2013 diffractometer with Cu Kα radiation [20].

Figure 3 summarizes relationships between the optical and electrical properties and the [D_2] value of the samples. The samples deposited with [D_2] ≤ 1.5 % were transparent, but that with [D_2] = 3.6 % was grayish. Optical transmittance T at the wavelength λ = 400, 600, and 800 nm of the samples deposited with [D_2] ≤ 1.5 % were high as ≥ 80 %. A low-T (≤ 40 %) was observed for the sample with [D_2] = 3.6 %. Hall mobility μ measured by van der Pauw method at room temperature (RT) of the samples with [D_2] ≤ 1 % stayed at a constant (≈55 $cm^2V^{-1}s^{-1}$), but that fell to ≈35 $cm^2V^{-1}s^{-1}$ and ≈10 $cm^2V^{-1}s^{-1}$ with increasing the [D_2] value to 1.5 % and 3.6 %, respectively. The μ value (≈55 $cm^2V^{-1}s^{-1}$) of the sample was almost the same as that reported (≈50 $cm^2V^{-1}s^{-1}$) by Koida et al. [1] for the hydrogen incorporated In_2O_3 films without any heat treatments. Carrier density N at RT of the samples demonstrated an inverse V-shaped behavior with the [D_2] value. Around [D_2] = 1 - 1.5 % the N value peaked at

≈7 × 10^{20} cm^{-3}, which is larger than the twice of that reported (≈3 × 10^{20} cm^{-3}) by Koida et al. [1]. In the hydrogen incorporated In_2O_3 films without any heat treatments, the carriers were supplied from oxygen vacancy [1]. We anticipated that oxygen vacancy plays the role of doubly charged impurities, and results in mobile carriers of the ITO films. Electrical resistivity ρ at 100, 200, and 280 K with van der Pauw configuration behaved similarly as a function of the [D_2] value. The ρ value became smaller from ≈5 × 10^{-4} Ωcm to ≈2.5 × 10^{-4} Ωcm with increasing [D_2] from 0 to 1 %, but at [D_2] ≥ 1.5 % that jumped in and stayed at ≈7 × 10^{-4} Ωcm. In present experiment, the sample deposited with [D_2] = 1 % was the most conducting. The resistivity of the [D_2] = 1 % sample by conventional four probe method reached to ≈1.5 × 10^{-4} Ωcm which is smaller than the value by van der Pauw method. Such a low resistivity for the sample without any heat treatments is almost the same to that (≤1.5 × 10^{-4} Ωcm) established well as low resistivity ITO films for the display applications fabricated with substrate heating in deposition and/or post annealing after the deposition. Furthermore the resistivity (≈1.5 × 10^{-4} Ωcm) of the [D_2] = 1 % sample matches up to the resistivity with N ≈7 × 10^{20} cm^{-3} expected from the Coulomb interaction between the electrons and the impurities [21].

As shown by the inset of Fig. 4, the samples showed doublet structure for the O 1*s* peak, which reflects the different charged states of oxygen in the solid. The suboxide-like peak at ≈532 eV corresponds to the hydroxyl-bonded oxygen [13]. The O 1*s* peak at ≈530 eV corresponds to the lattice oxygen. Relative intensity of the suboxide-like O 1*s* peak to the In 3*d* peak increased with increasing the [D_2] value, as seen in Fig. 4. Relative intensity of the lattice oxygen O 1*s* peak to the In 3*d* peak remained at almost constant (≈1). Protium contained in both residual gas of the sputtering chamber and adsorbed water from the ambient air during sample transfer forms a background peak for the hydroxyl-bonded oxygen. The background protium will give always a constant contribution in the physical property of the sample. Thus, background contributions should be distinguished from the aimed contributions due to the composition change in the plasma gas. Luo et al. [13] reported that the increase of hydroxyl-bonded oxygen is almost parallel to that of deuterium resided in the film.

The RBS spectra were simulated by using SIMNRA [22], and we saw the good agreements between the experiments and simulation [13]. Our RBS results on the ITO film on the glass substrate are consistent with those reported by Kumar et al. [23] except the existence of the Ba in the substrate and Ar in the ITO films. These elements might be segregated and implanted during the deposition, respectively. Oxygen content of the samples estimated from

RBS is shown in Fig. 5 as x in M_2O_x. Here, M represents the total of the metallic elements (In + Sn) in each sample. We can see that the ITO film with $[D_2] = 0$ % shows the stoichiometric composition. The introduction of deuterium into the plasma up to $[D_2] < 1$ % increases the oxygen deficiency, while further deuterium more than $[D_2] > 1$ % induces the excess of oxygen in the film. The sample with $[D_2] = 1$ % is the most oxygen deficient. From the Figs. 4 and 5, we can deduce that there are at least two competitive influences of the deuterium to the amount of oxygen in the sample, namely withdrawal of oxygen and formation of hydroxyl bond. In the low deuterium concentration region $[D_2] < 1$ % withdrawal of oxygen is dominant, whereas the formation of hydroxyl bond seems to be more effective in the deuterium rich region $[D_2] > 1$ %.

Limpijumnong et al. [4] pointed out that hydrogen atoms substituted for oxygen sites behave as donors. However we cannot determine experimentally the sites of deuterium atoms resided in ITO. Although we have no direct evidence of deuterium atoms substituted for oxygen sites, we confirmed that the concentration of the resided deuterium in the sample correlated almost linearly to the $[D_2]$ value, and further the change in the concentration of resided deuterium was almost parallel to that in the intensity of suboxide-like oxygen [13]. Therefore we considered that deuterium atoms primarily occupied the interstitial sites of ITO.

To see the influence of the two effects (withdrawal of oxygen and formation of hydroxyl bond), resistivity of the samples is plotted as a function of oxygen content in Fig. 6. It is noteworthy that there is a clear kink structure in the graph. As it seen, the increment rate of the resistivity with the oxygen content is large ($\Delta\rho/\Delta x = 11$) in the oxygen deficient region $x < 3$, while that in the excess of oxygen region ($x > 3$) is small ($\Delta\rho/\Delta x = 2$). From the above discussion, we can say that the oxygen deficiency ($3 - x$) correlates to the oxygen vacancy that acts as a double donor and largely decreases the resistivity. Present result is consistent to those reported [7-10], while it is in contradiction to those reported [2-4] concluding that oxygen vacancies are not responsible for free carriers in In_2O_3.

Figure 7 shows scanning TEM (STEM) images of the samples with $[D_2] = 1.5$ and 3.6 %. The dark field images and the In L x-ray maps revealed that the $[D_2] = 1.5$ % sample has monolithic structure with thickness of ≈150 nm, while the $[D_2] = 3.6$ % sample has porous structure with thickness of ≈130 nm. The film structure typical for the $[D_2] = 3.6$ % sample induces an enlargement of the effective surface area where water molecules can be adsorbed. The Ba L x-ray maps confirmed segregation of Ba to the substrate surface aforementioned in RBS.

Surface morphology was examined by a JEOL JSM-6360 scanning electron microscope (SEM) operated at the electron acceleration voltage of 15 kV. The SEM images shown in Fig. 8 demonstrate changes in surface morphology with [D_2]. An addition of deuterium by 1 % smoothed out surface corrugation. However further increase of deuterium gave rise to grain formation seen for the [D_2] = 1.5 % sample. Much more addition of deuterium to 3.6 % enhanced grain growth and agglomeration of the grains. The surface morphology by SEM strengthens the idea of enlargement of the effective surface area for the samples with [D_2] = 1.5 and 3.6 %. The samples showed the intense hydroxyl-bonded oxygen peak in XPS. Adsorbed water molecules can be transformed into In-$(OH)_{x \leq 3}$ species at the surface as illustrated in the lowest panel of Fig. 8, and then In-$(OH)_{x \leq 3}$ species intensify the hydroxyl-bonded oxygen peak. The calculated oxygen content x in M_2O_x, exceeding $x = 3$ for the samples with [D_2] = 1.5 and 3.6 % (Fig. 5), can be resulted from enhancement of absorption of water molecules.

As we expected before, the hydroxyl-bonded oxygen might play the role of scattering center for charge carriers, and then moderately enlarges the resistivity in the region of $x > 3$. However, we could not obtain simple relation between the carrier transport and the hydroxyl-bonded oxygen. The detail in the carrier transport of the hydrogen incorporated ITO films should be clarified in the region of excess of oxygen. Muonium was reported to form a shallow donor center with the activation energy of 47 ± 6 meV, and then hydrogen behaves as a shallow donor in In_2O_3 [2]. In the hydrogen-doped In_2O_3 films annealed in vacuum carriers are originated from singly charged impurities [1]. Therefore, Rutherford backscattering spectroscopy-elastic recoil detection analysis for the samples annealed in air and in vacuum is indispensable to clarify the origin of charge carriers of the hydrogen incorporated ITO films.

4. CONCLUSION

We employed XPS and RBS to examine contents of hydrogen and oxygen in the ITO films deposited in the plasma containing deuterium. The hydroxyl-bonded oxygen peak apparently grew with increasing the [D_2] value. Deuterium in the gas was incorporated into the solid at almost constant rate. We found no simple relation between the carrier transport and hydrogen at the interstitial site. The films deposited with [D_2] < 1 % and > 1 % exhibited oxygen deficiency and excess of oxygen than the stoichiometric composition, respectively. The most oxygen deficient film deposited with [D_2] = 1 % exhibited the lowest resistivity for the samples. Such oxygen deficiency correlated directly to oxygen vacancy playing the role of

double donor in ITO. Due to withdrawal of oxygen during the deposition of ITO film, hydrogen in plasma can be so effective for achieving lower resistivity without any heat treatments.

ACKNOWLEDGEMENTS

The authors thank Dr. H. Shimooka of Kyushu Institute of Technology for assistance, and Dr. H. Naramoto and the staff members of Tandem Accelerator Center in University of Tsukuba for RBS.

*Corresponding author. Tel.: +81-93-884-3310; Fax: +81-93-884-3300, E-mail address: kohiki@che.kyutech.ac.jp

REFERENCES

[1] T. Koida, H. Fujiwara, M. Kondo, Jpn. J. Appl. Phys. 46 (2007) L685.

[2] P. D. C. King, R. L. Lichti, Y. G. Celebi, J. M. Gil, R. C. Vilão, H. V. Alberto, J. P. Duarte, D. J. Payne, R. G. Egdell, I. McKenzie, C. F. McConville, S. F. J. Cox, T. D. Veal, Phys. Rev. B 80 (2009) 081201(R).

[3] S. Lany, A. Zunger, Phys. Rev. Lett. 98 (2007) 045501.

[4] S. Limpijumnong, P. Reunchan, A. Janotti, C. G. Van De Walle, Phys. Rev. B 80 (2009) 193202.

[5] C. G. Granqvist, A. Hultaker, Thin Solid Films 411 (2002) 1.

[6] H. Morikawa, M. Fujita, Thin Solid Films 359 (2000) 61.

[7] J. H. W. Dewit, J. Solid State Chem. 8 (1973) 142.

[8] J. H. W. Dewit, G. Vanunen, M. Lahey, J. Phys. Chem. Solids 38 (1977) 819.

[9] A. Dixit, C. Sudakar, R. Naik, V. M. Naik, G. Lawes, Appl. Phys. Lett. 95 (2009) 192105.

[10] T. Ohno, T. Kawahara, H. Tanaka, T. Kawai, M. Oku, K. Okada, S. Kohiki, J. J. Appl. Phys. 45 (2006) L957.

[11] S. Luo, K. Okada, S. Kohiki, F. Tsutsui, H. Shimooka, F. Shoji, Mater. Lett. 63 (2009) 641.

[12] J. Wallinga, W. M. Arnold Bik, A. M. Vredenberg, R. E. I. Schropp, W. F. van der Weg, J. Phys. Chem. B 102 (1998) 6219.

[13] S. Luo, S. Kohiki, K. Okada, A. Kohno, T. Tajiri, M. Arai, S. Ishii, D. Sekiba, M. Mitome, F. Shoji, ACS Appl. Mater. Interfaces 2 (2010) 663.

[14] E. G. Parada, P. Gonzalez, J. Serra, B. Leon, M. Perez-Amor, M. F. Da Silva, H. Wolters, J. C. Soares, J. Non-Cryst. Solids 187 (1995) 75.

[15] O. Bohnke, G. Frand, M. Fromm, J. Weber, O. Greim, Appl. Surf. Sci. 93 (1996) 45.

[16] M. Watamori, Nucl. Instrum. Meth. Phys. Res. B 249 (2006) 158.

[17] A. Inouye, S. Yamamoto, S. Nagata, M. Yoshikawa, T. Shikama, Nucl. Instrum. Meth. Phys. Res. B 266 (2008) 3381.

[18] F. L. Freire Jr., D. F. Franceschini, Thin Solid Films 293 (1993) 236.

[19] D. Sekiba, M. Horikoshi, S. Abe, S. Ishii, J. Appl. Phys. 106 (2009) 114912.

[20] S. Luo, S. Kohiki, K. Okada, F. Shoji, T. Shishido, Phys. Status Solidi A 207 (2010) 386.

[21] J. R. Bellingham, W. A. Phillips, C. J. Adkins, J. Mater. Sci. Lett. 11 (1992) 263.

[22] M. Mayer, SIMNRA, http://www.rzg.mpg.de/~mam/

[23] S. R. S. Kumar, P. Malar, T. Osipowicz, S. S. Banerjee, S. Kasiviswanathan, Nucl. Instrum.

Meth. Phys. Res. B 266 (2008) 1421.

FIGURE CAPTIONS

Fig. 1 Illustrative representation for the local structure of oxygen in In_2O_3. Upper panel: distorted tetrahedral In - O bonds have the bond lengths different from the average value [4]. Middle panel: deuterium resided at the interstitial site forms the hydroxyl bond OD_i in solid. Lower panel: oxygen vacancy V_O resulted from withdrawal of lattice-oxygen by deuterium radical during the deposition.

Fig. 2 Transmission electron micrograph of the cross-sectioned samples with $[D_2]$ = 0 (a), 1 (b), 1.5 (c), and 3.6 % (d). Insets: electron diffraction pattern of the samples.

Fig. 3 Optical transmittance T, Hall mobility μ, carrier density N, and electrical resistivity ρ of the samples as a function of $[D_2]$.

Fig. 4 Spectral intensity ratios of the O 1*s* to In 3*d* electrons of the samples as a function of $[D_2]$. Inset: O 1*s* spectra of the samples with $[D_2]$ of 0 (a) and 3.6 % (b). The arrows noted as $O_{Lattice}$ and $O_{Sub.}$ correspond to the O 1*s* peaks originated from the lattice oxygen and the hydroxyl-bonded oxygen, respectively. The arrows are guides for eye.

Fig. 5 Oxygen content *x* expressed as M_2O_x of the samples estimated from the RBS spectra as a function of $[D_2]$.

Fig. 6 Electrical resistivity ρ of the samples measured at 280 K as a function of oxygen content *x*. The broken lines are guides for eye.

Fig. 7 Dark field images (upper panel) and elemental maps of In *L* (middle panel) and Ba *L* x-rays (lower panel) by STEM for the sample with $[D_2]$ = 1.5 (left line) and 3.6 % (right line).

Fig. 8 SEM images of the samples with $[D_2]$ = 1 (a), 1.5 (b), and 3.6 % (c), and a sketch of grains at the surface of ITO film.

Fig. 1

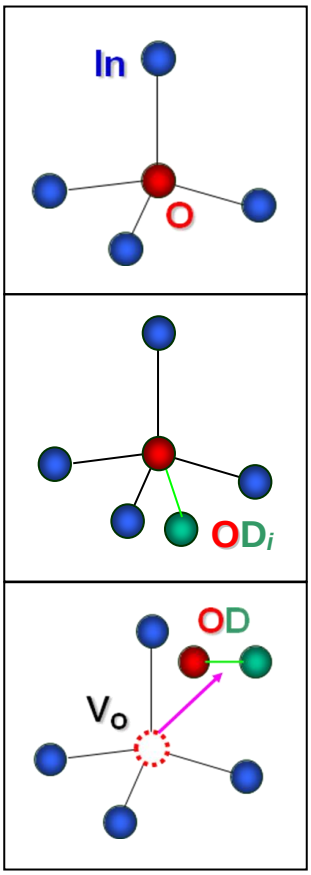

Fig. 2

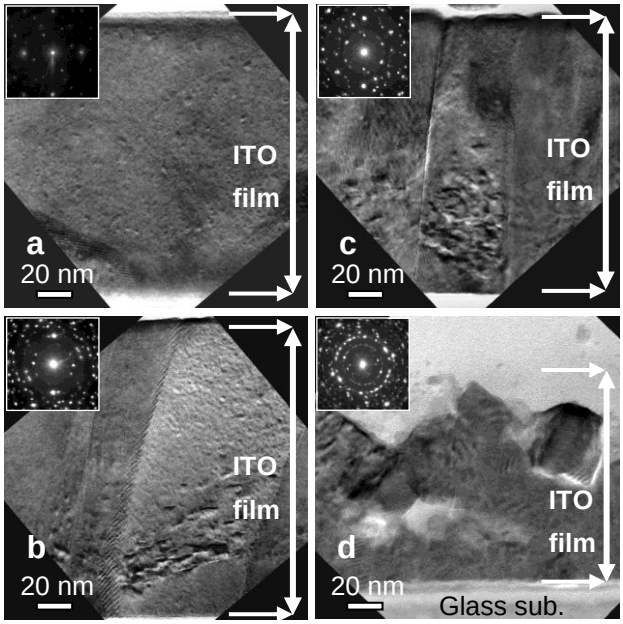
ITO
film
a
20 nm
ITO
film
c
20 nm
ITO
film
b
20 nm
ITO
film
d
20 nm
Glass sub.

Fig. 3

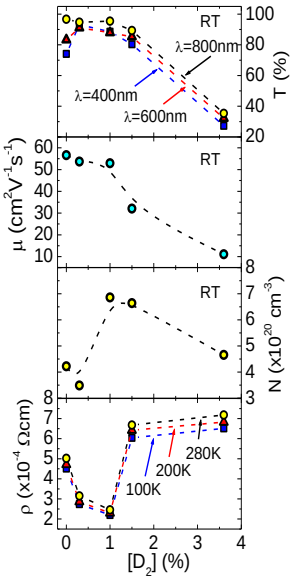
RT
λ=800nm
λ=400nm
λ=600nm
T (%)
RT
μ (cm²V⁻¹s⁻¹)
RT
N (x10²⁰ cm⁻³)
ρ (x10⁻⁴ Ωcm)
280K
200K
100K
[D2] (%)

Fig. 4

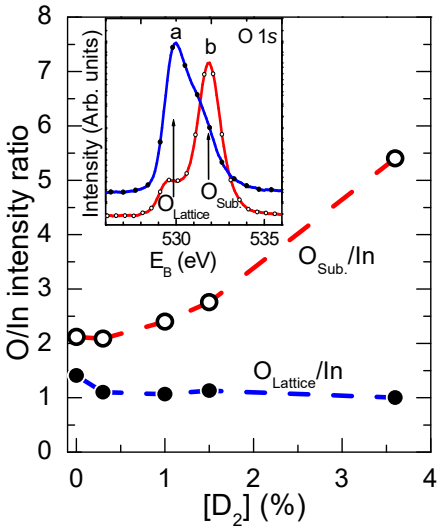
O/In intensity ratio
[D2] (%)
O Sub./In
O Lattice/In
Intensity (Arb. units)
E B (eV)
O 1s
a
b
O Lattice
O Sub.

Fig. 5

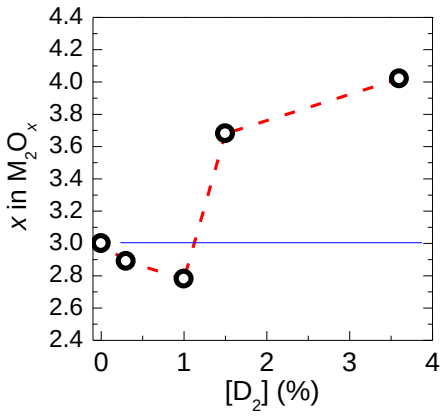

Fig. 6

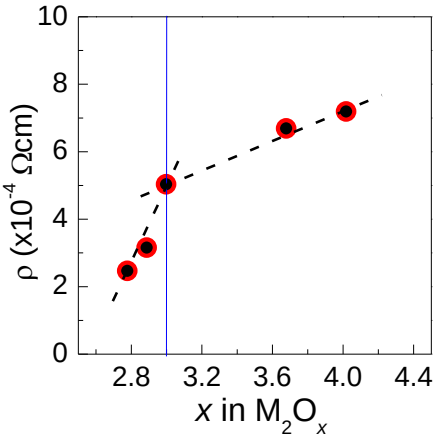

Fig. 7

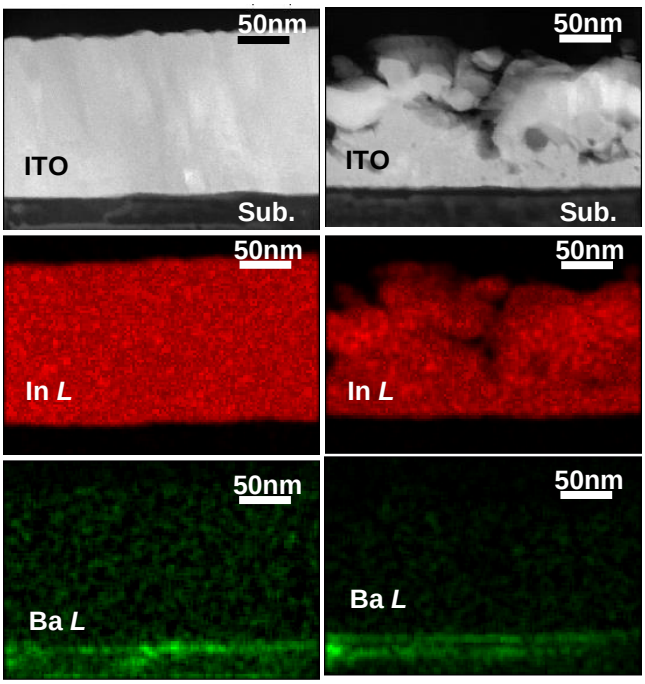

Fig. 8